A C^0 eight node finite element based on a shell theory

Comparison with the degenerated approach

Olivier Polit* ** — Maurice Touratier*

** LM2S - UPRES A 8007 - ENSAM 151 Bd de l'hopital - 75013 Paris*
*** Université Paris X - IUT - Dép. GMP 1 Chemin Desvallières F-92410 - Ville d'Avray*

ABSTRACT. *The development of C^0 eight node shell finite elements based upon the Reissner-Mindlin kinematics for geometrically and materially linear applications in structural mechanics is presented. Special attention is given ta the two ways of obtaining a shell finite element : shell theory and degenerated solid approach. We compare, with the same mechanical assumptions and the same finite element approximations, a new eight node semi-thick shell finite element based on a doubly curved shell theory (M2D) and an eight node finite element based on the degenerated approach (MDG). These two finite elements have the same five degrees of freedom (three translations and two rotations), use an explicit integration throughout the thickness and the same mcthodology to avoid shear and membrane locking.*

RÉSUMÉ. *Ce travail concerne le développement d'éléments finis C^0 à huit nœuds basés sur le modèle de Reissner-Mindlin pour l'analyse linéaire des coques. Notre attention se porte plus particulièrement sur l'utilisation d'un modèle de coque à double courbure par rapport à l'approche classique 3D dégénérée. Nous comparons un nouvel élément fini basé sur un modèle de coque (M2D) et un élément fini obtenu selon l'approche 3D dégénérée (MDG), basé sur les mêmes hypothèses mécaniques et les mêmes approximations élément fini. Ces deux éléments finis ont cinq degrés de liberté par nœud (trois translations et deux rotations), utilisent une intégration explicite suivant l'épaisseur et la même méthodologie pour corriger les phénomèmes de verrouillage.*

KEY WORDS : *shell theory, degenerated approach, finite element, shear locking, membrane locking, linear static tests.*

MOTS-CLÉS : *modèle de coque, approche 3D dégénérée, élément fini, verrouillage en cisaillement transverse, verrouillage en membrane, tests statiques linéaires.*

1. Introduction

Shell finite element developments have received considerable attention in the literature for many decades and many papers have been published. Some survey papers are available, see for instance References [Wem89], [Yan90], [Ide81], [Gil91], and a list of books, monographs, conference proceedings in Reference [Noo89].

This paper first deals with the choice of the shell model used to derive an efficient shell finite element. From a doubly curved shell theory, a new finite element is presented and compared with a finite element based on the degenerated solid approach using the same interpolations. In the literature, a discussion is always present about advantages and disadvantages of these two approaches for obtaining efficient numerical models (see for example References [Wem89, Gil91, Par89, Bue92]). These two C^0 shell finite elements have eight nodes with fully standard degrees of freedom for geometric and materially linear studies.

Since the eight node shell of Ahmad et al [Ahm70] [Coo74] where the degenerated approach was first introduced, few papers exist on new eight nodes. In References [Bat86] and [Hua86], eight nodes are introduced which are found less suitable than the new nine nodes presented by the same authors in [Buc93] and [Hua86]. Many papers have been published on four and nine node elements (see for instance References [Par89], [Pin89], [Sim89] and [And93]). This may be due to the fact that locking is even more pronounced for eight node elements than for four and nine types, and that eight nodes do not pass the constant curvature patch-test [Mac92]. In addition, the reduced integration is sufficient to correct the weakness of four and nine nodes introducing spurious mechanisms which must be controlled. Reduced integration does not in fact, permit completely avoiding the transverse shear locking for eight node finite elements [Hin86].

Objectives are to control the two numerical pathologies appearing when the shell becomes very thin :

transverse shear locking which is also present in the case of plate structures,

membrane locking which occurs only for some shell configurations called inextensional bending [Bel85], or non-inhibited pure bending [San89] from an asymptotic study of the response of elastic shells when the thickness tends towards zero.

A definition of the locking is given in [Bab92] as a non-uniformity of the convergence with respect to the thickness. The first attempt to avoid the locking phenomena in eight node shells has been proposed by Ahmad where reduced integration is used with a transverse shear correction factor. Other works on eight nodes based upon the degenerated approach are shown in [Bat86] and [Hua86]. In [Bat86], a mixed interpolation of tensorial components of the strains is in-

troduced, while in [Hua86] assumed strain interpolations are required with a partial reduced integration.

The originality of the present work is in the obtaining of a new eight node shell finite element with engineering degrees of freedom based on a doubly curved shell theory. It is based on a displacement variational formulation using differential geometry, tensorial calculations and an explicit integration throughout the thickness. It seems there are no other published works on C^0 eight node shell finite elements based on a curvilinear approach with standard engineering degrees of freedom. In addition, a comparison with an eight node finite element based on the degenerated approach using the same finite element approximation is conducted. This finite element approximation has been proposed in the assumed natural strain context.

The next section allows us to present succintly some geometric features for shells and we introduce the shell models (kinematics and strain tensor) in the third section. Section four is dedicated to the finite element approximation. Finally these finite elements have been evaluated on standard tests : membrane tests, Scordelis-Lo roof (cylindrical panel), pinched cylinder and hemispherical shell.

2. Geometric considerations

To define geometric and mechanical properties of the shell, three different base vectors are introduced :

i- *global cartesian base vectors* $(\vec{e}_1, \vec{e}_2, \vec{e}_3)$ used to define the geometry of the shell,

ii- *local curvilinear base vectors* $(\vec{a}_1, \vec{a}_2, \vec{a}_3)$: the vectors $(\vec{a}_1, \vec{a}_2)$ define the tangent plane of the shell middle surface while $\vec{a}_3$ is associated with the normal direction. These base vectors will be described later,

iii- *local orthonormal curvilinear base vectors* $(\vec{t}_1, \vec{t}_2, \vec{t}_3)$: we prescribe $\vec{t}_3 = \vec{a}_3$. In this work, the definition of these base vectors is classic (see [Bat92], p. 237).

A map $\vec{r}_0$ is introduced to define the shell middle surface $\bar{S}$, and the shell thickness is given by the function $e(\xi^1, \xi^2)$. Therefore an arbitrary point of the shell is given by :

$$\vec{r}(\xi^1, \xi^2, \xi^3) = \vec{r}_0(\xi^1, \xi^2) + \xi^3 \vec{a}_3 \quad \text{where} \quad -\frac{e(\xi^1, \xi^2)}{2} \leq \xi^3 \leq \frac{e(\xi^1, \xi^2)}{2} \tag{1}$$

For a point on the shell middle surface, covariant base vectors are usually obtained as follows :

$$\vec{a}_\alpha = \vec{r}_0(\xi^1,\xi^2)_{,\alpha} \quad ; \quad \vec{a}_3 = \frac{\vec{a}_1 \times \vec{a}_2}{||\vec{a}_1 \times \vec{a}_2||} = \vec{t}_3 \tag{2}$$

In equation (2) and further on, latin indices $i, j, \ldots$ take their values in the set $\{1,2,3\}$ while greek indices $\alpha, \beta, \ldots$ take their values in the set $\{1,2\}$. The summation convention on repeated indices and the classic notation $(\ )_{,\alpha} = \frac{\partial(\ )}{\partial \xi^\alpha}$ are used.

For any point of the shell, covariant base vectors are now deduced as :

$$\vec{g}_\alpha = \vec{r}(\xi^1,\xi^2,\xi^3)_{,\alpha} = (\delta_\alpha^\beta - \xi^3 b_\alpha^\beta)\vec{a}_\beta = \mu_\alpha^\beta \vec{a}_\beta \quad \text{and} \quad \vec{g}_3 = \vec{a}_3 = \vec{t}_3 \tag{3}$$

The mixed tensor m_α^β must also be introduced and is defined by the relation :

$$m_\alpha^\beta = (\mu^{-1})_\alpha^\beta = \frac{1}{\mu}\{\delta_\alpha^\beta + \xi^3(b_\alpha^\beta - 2H\delta_\alpha^\beta)\} \tag{4}$$

where $\mu = det(\mu_\alpha^\beta) = 1 - 2H\xi^3 + (\xi^3)^2 K$; $H = \frac{1}{2}tr(b_\alpha^\beta)$; $K = det(b_\alpha^\beta)$.

Finally, the base vector change can be written under the following matrix relations :

$$\begin{bmatrix} \vec{t}_1 \\ \vec{t}_2 \end{bmatrix} = [TA] \begin{bmatrix} \vec{a}_1 \\ \vec{a}_2 \end{bmatrix} \text{ with } [TA] = \begin{bmatrix} \vec{a}^1.\vec{t}_1 & \vec{a}^2.\vec{t}_1 \\ \vec{a}^1.\vec{t}_2 & \vec{a}^2.\vec{t}_2 \end{bmatrix} \tag{5}$$

$$\begin{bmatrix} \vec{t}_1 \\ \vec{t}_2 \end{bmatrix} = [TG] \begin{bmatrix} \vec{g}_1 \\ \vec{g}_2 \end{bmatrix} \text{ with } [TG] = \begin{bmatrix} \vec{g}^1.\vec{t}_1 & \vec{g}^2.\vec{t}_1 \\ \vec{g}^1.\vec{t}_2 & \vec{g}^2.\vec{t}_2 \end{bmatrix} \tag{6}$$

Introducing equation (3) into (6) and using (5), we obtain $[TG]$ as a function of $[TA]$ and curvature tensor components b_α^β :

$$[TG] = \frac{1}{\mu}\left([TA] + \xi^3 [TA]\,[Ibm]\right) \qquad \text{with} \qquad [Ibm] = \begin{bmatrix} -b_2^2 & b_2^1 \\ b_1^2 & -b_1^1 \end{bmatrix} \tag{7}$$

3. Strain expression for the curvilinear shell model

3.1. *Displacement vector*

The three-dimensional displacement vector is defined as follows :

$$\vec{u} = \vec{v} + \xi^3 \vec{\beta} \tag{8}$$

In this expression, $\vec{u}$ is the displacement vector of any point of the shell, while $\vec{v}$ is the displacement vector of any point of the shell middle surface and $\vec{\beta}$ is the rotation vector associated with the normal fiber of the shell.

The covariant components of displacement and rotation vectors with respect to the two curvilinear base vectors previously introduced can be expressed as :

$$\begin{aligned} \vec{v} &= \bar{v}_i \vec{a}^i = v_i \vec{t}^i \\ \vec{\beta} &= \bar{\beta}_\alpha \vec{a}^\alpha = \beta_\alpha \vec{t}^\alpha \end{aligned} \tag{9}$$

From the definition of the normal vector, it should be notice that we have $v_3 = \bar{v}_3$.

3.2. *Strain tensor*

The strain tensor can be defined by its covariant components using either $\vec{a}^i$ or $\vec{t}^i$ curvilinear bases as :

$$\epsilon(\vec{u}) = \bar{\epsilon}_{ij}(\vec{a}^i \otimes \vec{a}^j) = \epsilon_{ij}(\vec{t}^i \otimes \vec{t}^j) \tag{10}$$

After some algebraic transformations, expressions of covariant components of the strain tensor can be written as :

$$\left\{ \begin{array}{lcl} 2\bar{\epsilon}_{\alpha\beta} & = & \dfrac{1}{\mu}\{\bar{\epsilon}^0{}_{\alpha\beta} + \bar{\epsilon}^0{}_{\beta\alpha} + \xi^3\{(b^\lambda_\beta - 2H\delta^\lambda_\beta)\bar{\epsilon}^0{}_{\alpha\lambda} + (b^\lambda_\alpha - 2H\delta^\lambda_\alpha)\bar{\epsilon}^0{}_{\beta\lambda} + \\ & & \bar{\epsilon}^1{}_{\alpha\beta} + \bar{\epsilon}^1{}_{\beta\alpha}\} + (\xi^3)^2\{(b^\lambda_\beta - 2H\delta^\lambda_\beta)\bar{\epsilon}^1{}_{\alpha\lambda} + (b^\lambda_\alpha - 2H\delta^\lambda_\alpha)\bar{\epsilon}^1{}_{\beta\lambda}\}\} \\ \bar{\gamma}_{\alpha 3} & = & \dfrac{1}{\mu}\{\bar{\gamma}^0{}_{\alpha 3} + \xi^3(b^\lambda_\alpha - 2H\delta^\lambda_\alpha)\bar{\gamma}^0{}_{\lambda 3}\} \\ \bar{\epsilon}_{33} & = & 0 \end{array} \right. \tag{11}$$

where

$$\left\{ \begin{array}{lcl} \bar{\epsilon}^0{}_{\alpha\beta} & = & \bar{v}_{\alpha|\beta} - b_{\alpha\beta} v_3 \\ \bar{\epsilon}^1{}_{\alpha\beta} & = & \bar{\beta}_{\alpha|\beta} \\ \bar{\gamma}^0{}_{\alpha 3} & = & \bar{\beta}_\alpha + v_{3|\alpha} + b^\gamma_\alpha \bar{v}_\gamma \end{array} \right. \tag{12}$$

Covariant components ϵ_{ij} of the strain tensor introduced in equation (10) can be derived from equation (11) by means of a classic tensorial transformation.

3.3. *Matrix expression of the strain tensor*

Matrix expressions of the strain tensor associated with the pure bidimensional shell model are now given.

In-plane strains

The matrix form of the in-plane strain components deduced from equations (11) are computed with respect to the base vectors $\vec{t}^i$ as :

$$[\epsilon] = \begin{bmatrix} \epsilon_{11} \\ \epsilon_{22} \\ \gamma_{12} \end{bmatrix} = [TT] \begin{bmatrix} \bar{\epsilon}_{11} \\ \bar{\epsilon}_{22} \\ \bar{\gamma}_{12} \end{bmatrix} \tag{13}$$

Relation $\gamma_{12} = \epsilon_{12} + \epsilon_{21}$ is of course included in equation (13), and $[TT]$ is the tensorial transformation matrix between the two curvilinear bases, see equation (10). Its expression is :

$$[TT] = \begin{bmatrix} (\vec{a}^1.\vec{t}_1)^2 & (\vec{a}^2.\vec{t}_1)^2 & (\vec{a}^1.\vec{t}_1)(\vec{a}^2.\vec{t}_1) \\ (\vec{a}^1.\vec{t}_2)^2 & (\vec{a}^2.\vec{t}_2)^2 & (\vec{a}^1.\vec{t}_2)(\vec{a}^2.\vec{t}_2) \\ 2(\vec{a}^1.\vec{t}_1)(\vec{a}^1.\vec{t}_2) & 2(\vec{a}^2.\vec{t}_1)(\vec{a}^2.\vec{t}_2) & (\vec{a}^1.\vec{t}_1)(\vec{a}^2.\vec{t}_2) + (\vec{a}^1.\vec{t}_2)(\vec{a}^2.\vec{t}_1) \end{bmatrix} \tag{14}$$

The second matrix in the right member of equation (13) can be written in the following form :

$$\begin{bmatrix} \bar{\epsilon}_{11} \\ \bar{\epsilon}_{22} \\ \bar{\gamma}_{12} \end{bmatrix} = \frac{1}{\mu} \left([G1] \left[\bar{E}^0\right] + \xi^3 \left([G2] \left[\bar{E}^0\right] + [G1] \left[\bar{E}^1\right] \right) + (\xi^3)^2 [G2] \left[\bar{E}^1\right] \right) \tag{15}$$

where the matrices $[G1]$ and $[G2]$ are defined by :

$$[G1] = \begin{bmatrix} 1 & 0 & 0 & 0 \\ 0 & 1 & 0 & 0 \\ 0 & 0 & 1 & 1 \end{bmatrix} \qquad [G2] = \begin{bmatrix} -b_2^2 & 0 & b_1^2 & 0 \\ 0 & -b_1^1 & 0 & b_2^1 \\ b_2^1 & b_1^2 & -b_1^1 & -b_2^2 \end{bmatrix}$$

and the generalized strain matrices are :

$$\left[\bar{E}^0\right]^T = \begin{bmatrix} \bar{\epsilon}^0{}_{11} & \bar{\epsilon}^0{}_{22} & \bar{\epsilon}^0{}_{12} & \bar{\epsilon}^0{}_{21} \end{bmatrix} \quad ; \quad \left[\bar{E}^1\right]^T = \begin{bmatrix} \bar{\epsilon}^1{}_{11} & \bar{\epsilon}^1{}_{22} & \bar{\epsilon}^1{}_{12} & \bar{\epsilon}^1{}_{21} \end{bmatrix}$$

Transverse shear strains

A matrix expression for the transverse shear strains is derived from the above method. We obtain :

$$[\gamma] = \begin{bmatrix} \gamma_{13} \\ \gamma_{23} \end{bmatrix} = \frac{1}{\mu} [TA] \left([Id] + \xi^3 [Ibm]^T \right) \left[\bar{G}^0\right] \tag{16}$$

$$\text{with } \left[\bar{G}^0\right]^T = \begin{bmatrix} \bar{\gamma}^0{}_{13} & \bar{\gamma}^0{}_{23} \end{bmatrix}$$

Expressions (15) and (16) will be very useful later during the finite element approximations of the shell models, and especially to help carefully interpolate membrane and transverse shear strains to avoid locking phenomena.

3.4. About the degenerated approach

The strain components for the degenerated approach can be derived using the matrix expressions obtained previously for the curvilinear shell model.

For the degenerated approach, the displacement vectors $\vec{u}$ introduced in (8) differ from (9) only by the definition of the displacement vector $\vec{v}$ of a point of the shell middle surface. This displacement is expressed with respect

to the cartesian base vectors $\vec{e}_i$, while for the pure bidimensional shell model we use the curvilinear orthonormal base vectors $\vec{t}_i$. We therefore have for the degenerated approach :

$$\vec{v} = v_i \vec{e}_i \tag{17}$$

The matrix expression of the strain is then given by equations (15) and (16), using the expression of the generalized strain for the degenerated approach given by :

$$\begin{aligned}
\left[\bar{E}^0\right]^T &= \left[\begin{array}{cccc} \bar{e}^0{}_{11} & \bar{e}^0{}_{22} & \bar{e}^0{}_{12} & \bar{e}^0{}_{21} \end{array}\right] \\
\left[\bar{E}^1\right]^T &= \left[\begin{array}{cccc} \bar{e}^1{}_{11} & \bar{e}^1{}_{22} & \bar{e}^1{}_{12} & \bar{e}^1{}_{21} \end{array}\right] \\
\left[\bar{G}^0\right]^T &= \left[\begin{array}{cc} \bar{g}^0{}_{13} & \bar{g}^0{}_{23} \end{array}\right]
\end{aligned} \quad \text{with} \quad \left\{\begin{array}{lcl}
\bar{e}^0{}_{\alpha\gamma} &=& \vec{a}_\alpha . \vec{v}_{,\gamma} \\
\bar{e}^1{}_{\alpha\gamma} &=& \vec{a}_\alpha . \vec{\beta}_{,\gamma} \\
\bar{g}^0{}_{\alpha 3} &=& \vec{a}_\alpha . \vec{\beta} + \vec{a}_3 . \vec{v}_{,\alpha}
\end{array}\right. \tag{18}$$

This last expression (18) must be compared with equation (12) for the curvilinear shell model. Coupling due to curvature in $\bar{\epsilon}_{\alpha\beta}{}^0$ and $\bar{\gamma}_{\alpha 3}{}^0$ (see equation (12)) is evident while for the degenerated approach (see equation (18)) this coupling is included in the scalar products.

4. Finite element approximation

4.1. The weak form of the boundary-value problem for shells

A shell is deduced from a middle surface S and a thickness e as defined above. V is the space occupied by the shell and ∂V_F is its boundary part where loads are prescribed.

Let σ denote the Cauchy stress tensor, $\vec{f}$ and $\vec{F}$ being respectively the prescribed body and surface force vectors. Because the shell thickness is small in comparison with the other dimensions, the normal transverse stress is assumed to be zero.

Using the matrix notation introduced in section 3., the principle of virtual power for a linearly elastostatic problem is given by :

Find $\vec{u} \in U$ so that :

$$\int_V [D^*]^T [\sigma] dV = \int_V [u^*]^T [f] dV + \int_{\partial V_F} [u^*]^T [F] d\partial V \ , \quad \forall \vec{u}^* \in U^* \tag{19}$$

where $[u^*]$ is the matrix notation of the virtual velocity vector $\vec{u}^*$ and $[D^*]$ is the matrix notation of the virtual strain rate tensor components D^*_{ij}. $[\sigma]$, $[f]$, $[F]$ are the matrix notations associated respectively with the Cauchy stress tensor, prescribed body and surface force vectors. The two functional spaces U and U^* are respectively the space of kinematically admissible displacements and the space of virtual velocities.

Then, if we let C_{ijkl} be the elastic constants for an homogeneous material, and [C] its corresponding matrix notation, we have :

$$[\sigma] = [C] \begin{bmatrix} [\epsilon] \\ [\gamma] \end{bmatrix} \text{ with } [\sigma]^T = \begin{bmatrix} \sigma_{11} & \sigma_{22} & \sigma_{12} & \sigma_{13} & \sigma_{23} \end{bmatrix}$$

$$[C] = \begin{bmatrix} [C_\epsilon] & [0] \\ [0] & [C_\gamma] \end{bmatrix} \tag{20}$$

$$[D^*]^T = \begin{bmatrix} [\epsilon^*]^T & [\gamma^*]^T \end{bmatrix} \text{ with } \begin{cases} [\epsilon^*]^T = \begin{bmatrix} \epsilon^*_{11} & \epsilon^*_{22} & \gamma^*_{12} \end{bmatrix} \\ [\gamma^*]^T = \begin{bmatrix} \gamma^*_{13} & \gamma^*_{23} \end{bmatrix} \end{cases}$$

In equation (20), $[C]$ is the matrix associated with the two-dimensional constitutive law which takes into account the assumption of zero transverse normal stress.

Development of the left member of the functional defined in equation (19) can now be made by splitting this last equation into its in-surface strain and its transverse shear strain parts. It follows that :

$$\int_V [D^*]^T [\sigma] dV = \int_S \int_{-e/2}^{e/2} \left([\epsilon^*]^T [C_\epsilon] [\epsilon] + [\gamma^*]^T [C_\gamma] [\gamma] \right) \mu d\xi^3 dS \tag{21}$$

From equations (13) and (15), an explicit integration through the thickness of the shell can be performed, using second order series expansion for $1/\mu$. Finally, the following integrated matrices are at most of the third order with respect to the thickness e and we denote :

$$[C_\epsilon \alpha] = \int_{-e/2}^{e/2} \frac{(\xi^3)^\alpha}{\mu} [C_\epsilon] \, d\xi^3 \text{ with } \alpha = 0, 1, 2. \tag{22}$$

As for the in-surface strains above, an explicit integration throughout the thickness is performed for the transverse shear part and gives us the following matrices :

$$[C_\gamma \alpha] = \int_{-e/2}^{e/2} \frac{(\xi^3)^\alpha}{\mu} [C_\gamma] \, d\xi^3 \text{ with } \alpha = 0, 1. \tag{23}$$

4.2. The discrete form of the boundary-value problem for shells

To solve equation (19), finite-dimensional approximations of the spaces U and U^* must be defined. We denote U^h and U^{*h} these finite-dimensional subspaces, where the superscript h refers to a discretisation of the middle surface which contains n_{elt} finite elements, denoted by $(\Omega_e)_{e=1,n_{elt}}$.

Let us now consider an element Ω_e of the middle surface's discretisation. The element has eight nodes (see Figure 1) and is mapped from the standard isoparametric quadrilateral element (denoted Ω_{ref}) by a one-to-one and onto mapping. Problem (19) can be written in the following form.

Find $\vec{u}^h \in U^h$ so that :

$$\sum_{e=1}^{n_{el}} a(\vec{u}^h, \vec{u}^{*h})_{|\Omega_e} = \sum_{e=1}^{n_{el}} f(\vec{u}^{*h})_{|\Omega_e} + \sum_{e=1}^{n_{el}} F(\vec{u}^{*h})_{|\partial\Omega_e} , \quad \forall \vec{u}^{*h} \in U^{*h} \tag{24}$$

with

$$\begin{aligned} a(\vec{u}^h, \vec{u}^{*h})_{|\Omega_e} = \int_{\Omega_e} & \left(\left[\bar{E}^{0*h}\right]^T ([TG11C_\epsilon 0] + [TG12C_\epsilon 1] + [TG21C_\epsilon 1] \right. \\ & + [TG22C_\epsilon 2]) \left[\bar{E}^{0h}\right] + \left[\bar{E}^{1*h}\right]^T [TG11C_\epsilon 2] \left[\bar{E}^{1h}\right] + \\ & \left[\bar{E}^{0*h}\right]^T ([TG11C_\epsilon 1] + [TG12C_\epsilon 2] + [TG21C_\epsilon 2]) \left[\bar{E}^{1h}\right] + \\ & \left[\bar{E}^{1*h}\right]^T ([TG11C_\epsilon 1] + [TG12C_\epsilon 2] + [TG21C_\epsilon 2]) \left[\bar{E}^{0h}\right] + \\ & \left[\bar{G}^{0*h}\right]^T \left([TA]^T [C_\gamma 0] [TA] + [TA]^T [C_\gamma 1] [TA] [Ibm]^T + \right. \\ & \left. \left. [Ibm] [TA]^T [C_\gamma 1] [TA] \right) \left[\bar{G}^{0h}\right] \right) \sqrt{a} d\xi^1 d\xi^2 \end{aligned} \tag{25}$$

where $\left[\bar{E}^{0*h}\right]$ (respectively $\left[\bar{E}^{1*h}\right]$) has the same expression as $\left[\bar{E}^{0h}\right]$ (respectively $\left[\bar{E}^{1h}\right]$) for the virtual velocity vector, and where it has been denoted :

$$[TGmnC_\epsilon\alpha] = [Gm]^T [TT]^T [C_\epsilon\alpha] [TT] [Gn] \quad \text{with} \quad \begin{matrix} (m,n) \in \{1,2\}^2 \\ \alpha = 0,1,2. \end{matrix}$$

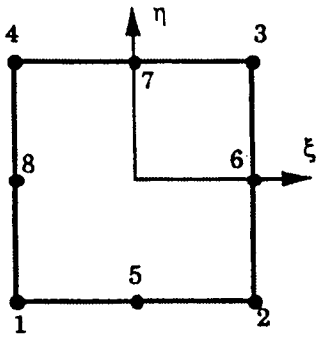

Figure 1: *The reference closed domain Ω_{ref} in isoparametric co-ordinates (ξ, η)*

For each element, the geometry is deduced from the classic Serendipity interpolation as :

$$\begin{Bmatrix} {x_1}^h(\xi,\eta) \\ {x_2}^h(\xi,\eta) \\ {x_3}^h(\xi,\eta) \end{Bmatrix} = \sum_{i=1}^{8} N_i(\xi,\eta) \begin{Bmatrix} x_{1i} \\ x_{2i} \\ x_{3i} \end{Bmatrix} \tag{26}$$

where $N_i(\xi,\eta)$ are quadratic Serendipity interpolation functions and x_{1i} (for example) is the first cartesian co-ordinate of the ith node of the element. The reduced co-ordinates are classically defined by $(\xi,\eta) \in [-1,1]^2$, see Figure 1.

According to the above notation, the reduced co-ordinates (ξ,η) can be seen as a local curvilinear co-ordinate system (ξ^1,ξ^2) defined for each element. All the differential geometric entities presented in Section 2. are then deduced from equations (26). On each elementary domain Ω_e and without loss of generality, metric and curvatures are supposed to be constant. Therefore, classical derivatives can be substituted for surface covariant derivatives in equation (12).

Let $[ql_e]$ be the local vector of degrees of freedom (dof) for an element Ω_e. Since the C^0 element has eight nodes, this vector is defined by :

$$[ql_e]^T = [\ v_{11}\quad v_{21}\quad v_{31}\quad \beta_{11}\quad \beta_{21}\quad \dots\quad v_{18}\quad v_{28}\quad v_{38}\quad \beta_{18}\quad \beta_{28}\ ] \tag{27}$$

where the second lowerscript indicates the node number. The vector $[ql^*{}_e]$ associated with the virtual displacement vector is defined in the same way.

From equation (25), the elementary stiffness matrix denoted $[K_e]$ is defined by :

$$a(\vec{u}^h,\vec{u}^{*h})_{|\Omega_e} = [ql^*{}_e]^T[K_e][ql_e] \tag{28}$$

Interpolations for in-surface displacement and rotation components with respect to the local orthonormal vectors $\vec{t}_i$ are given by :

$$\begin{aligned} v_\alpha{}^h &= \sum_{i=1}^{8} N_i(\xi,\eta) v_{\alpha i} \\ \beta_\alpha{}^h &= \sum_{i=1}^{8} N_i(\xi,\eta) \beta_{\alpha i} \end{aligned} \tag{29}$$

From equation (9) and using the above interpolations (29), any component of in-surface displacement or rotation $\bar{p}_\alpha{}^h$ evaluated at a point (ξ_K,η_K) is given by :

$$\bar{p}_\alpha{}^h(\xi_K,\eta_K) = \sum_{i=1}^{8} N_i(\xi_K,\eta_K)\left\{p_{1i}(\vec{a}_{\alpha K}.\vec{t}_{1i}) + p_{2i}(\vec{a}_{\alpha K}.\vec{t}_{2i})\right\} \tag{30}$$

It must be notice in equation (30) that scalar products are defined between local vector $\vec{a}_\alpha$ evaluated at the calculation point K, and local orthonormal vector $\vec{t}_\alpha$ calculated at nodes i.

4.3. Strain approximation

In order to lighten expressions for strains, the superscript h is henceforth omitted and reduced co-ordinates (ξ,η) are introduced as indexes for displacement,

rotation and strain components. We then have :

$$\begin{array}{ll} v_\xi = \bar{v}_1 & v_\eta = \bar{v}_2 \\ \beta_\xi = \bar{\beta}_1 & \beta_\eta = \bar{\beta}_2 \\ \epsilon^0{}_{\xi\xi} = \bar{\epsilon}^0{}_{11} & \epsilon^0{}_{\eta\eta} = \bar{\epsilon}^0{}_{22} \\ \epsilon^0{}_{\xi\eta} = \bar{\epsilon}^0{}_{12} & \epsilon^0{}_{\eta\xi} = \bar{\epsilon}^0{}_{21} \\ \gamma^0{}_\xi = \bar{\gamma}^0{}_{13} & \gamma^0{}_\eta = \bar{\gamma}^0{}_{23} \end{array} \tag{31}$$

To avoid shear and membrane locking, the strain interpolation will be modified. Thus, we split strain into its classic bending, transverse shear and membrane parts.

4.3.1. Bending strain interpolations

Bending strain interpolations are directly deduced from the Serendipity interpolation of rotation components. Using matrix notations, the bending strain components may be written as :

$$\left[\bar{E}^1\right] = [BF]\,[ql_e] \tag{32}$$

where the matrix $[BF]$ has a $(4, 40)$ dimension and the following form :

$$[BF] = \left[\ [BF_1] \quad \ldots \quad [BF_8]\ \right]$$

Each matrix $[BF_i]$ of a $(4, 5)$ dimension is usually given by :

$$[BF_i] = \begin{bmatrix} 0 & 0 & 0 & -(\vec{a}_1.\vec{t}_{2i})\ N_{i,\xi} & (\vec{a}_1.\vec{t}_{1i})\ N_{i,\xi} \\ 0 & 0 & 0 & -(\vec{a}_2.\vec{t}_{2i})\ N_{i,\eta} & (\vec{a}_2.\vec{t}_{1i})\ N_{i,\eta} \\ 0 & 0 & 0 & -(\vec{a}_1.\vec{t}_{2i})\ N_{i,\eta} & (\vec{a}_1.\vec{t}_{1i})\ N_{i,\eta} \\ 0 & 0 & 0 & -(\vec{a}_2.\vec{t}_{2i})\ N_{i,\xi} & (\vec{a}_2.\vec{t}_{1i})\ N_{i,\xi} \end{bmatrix}$$

In this matrix expression, the scalar product is between vector $\vec{a}_\alpha$ calculated at the integration points and vector $\vec{t}_\delta$ evaluated at the node i (see equation (30)).

4.3.2. Transverse shear strain interpolations

An efficient method for avoiding transverse shear locking has been presented in Reference [Pol94] and applied to an eight-node plate finite element. This method is extended here to shell structures. From equations (16), finite element approximation of the following matrix $[\bar{G}^0]$ must be defined :

$$\left[\bar{G}^0\right] = \begin{bmatrix} \gamma^0{}_\xi \\ \gamma^0{}_\eta \end{bmatrix} = \begin{bmatrix} \beta_\xi + v_{3,\xi} + b^1_1 v_\xi + b^2_1 v_\eta \\ \beta_\eta + v_{3,\eta} + b^1_2 v_\xi + b^2_2 v_\eta \end{bmatrix} \tag{33}$$

Hereafter, the methodology is briefly recalled. The first two steps permit defining the interpolation of v_3 and the two others are then dedicated to the interpolation of the two transverse shear strain components.

- a quadratic interpolation for $\beta_\xi, \beta_\eta, v_\xi, v_\eta$ is used, hence a cubic interpolation is chosen for v_3 in order to have same order polynomia following the ξ-direction for ${\gamma^0}_\xi$ (resp. η-direction for ${\gamma^0}_\eta$) for all the functions present in equation (33). We then introduce four degrees of freedom (one at each mid-side node) to the eight initial ones : $(v_{3,\xi})_5$, $(v_{3,\eta})_6$, $(v_{3,\xi})_7$, $(v_{3,\eta})_8$.

- constraining tangential shear strains to be linear along each edge of the element, these derivative degrees of freedom are expressed as functions of the standard ones given by equation (27). Interpolation for v_3 is then deduced and will be useful when computing ${\gamma^0}_\alpha$ following the strain substitution method.

- to get consistent interpolation for transverse shear strain components, we must interpolate ${\gamma^0}_\xi$ (resp. ${\gamma^0}_\eta$) in the polynomial space associated with the base $\{1, \xi, \eta, \xi\eta, \eta^2\}$ ($\{1, \xi, \eta, \xi\eta, \xi^2\}$) which is the common monomial term set of the polynomial bases for each displacement/rotation interpolation in equation (33). Five points are then needed to interpolate transverse shear strain components. The selected points, denoted $I_1, \ldots I_5$ for ${\gamma^0}_\xi$ and $J_1, \ldots J_5$ for ${\gamma^0}_\eta$, are shown in Figure 2 according to numerical efficiency of the element response in the case of distorted meshes.

- thus, ${\gamma^0}_\xi(I_i)$ and ${\gamma^0}_\eta(J_i)$ for $i = 1, 5$ must be calculated using equation (33) from interpolation defined in equation (30) for in-surface displacements/rotations and the above cubic one for v_3. Values of the transverse shear strain components on the whole reference domain are deduced using extrapolation functions.

Finally, the matrix expression of the transverse shear strain components is given by :

$$[\tilde{G}^0] = [BC]\,[PC]\,[ql_e] \tag{34}$$

with

$$\left[\ {\gamma^0}_\xi(I_1) \quad \ldots \quad {\gamma^0}_\xi(I_5) \quad {\gamma^0}_\eta(J_1) \quad \ldots \quad {\gamma^0}_\eta(J_5)\ \right]^T = [PC]\,[ql_e]$$

and

$$[BC] = \begin{bmatrix} C\xi_{I1}(\xi,\eta) & \ldots & C\xi_{I5}(\xi,\eta) & 0 & \ldots & 0 \\ 0 & \ldots & 0 & C\eta_{J1}(\xi,\eta) & \ldots & C\xi_{I5}(\xi,\eta) \end{bmatrix}$$

In these expressions, I_{1-5} and J_{1-5} indicate the points (see Figure 2) where transverse shear strain components are computed from equation (30) and corresponding interpolations defined previously. $C\xi_I, C\eta_J$ are extrapolation functions given in Reference [Pol94].

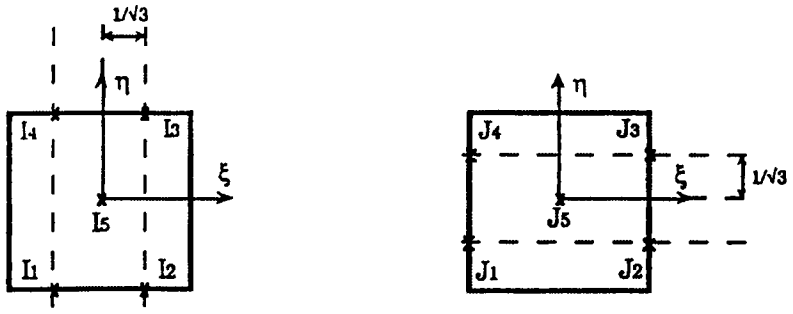

Figure 2: *Point locations where the shear strain components* γ_ξ, γ_η *are evaluated*

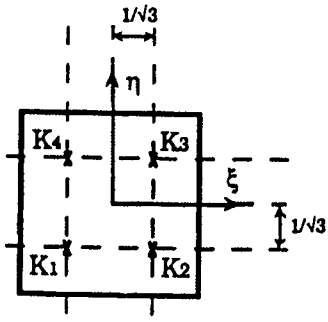

Figure 3: *Point locations where the membrane strain components* $\epsilon^0_{\xi\xi}, \epsilon^0_{\eta\eta}, \epsilon^0_{\xi\eta}, \epsilon^0_{\eta\xi}$ *are evaluated*

4.3.3. Membrane strain interpolations

The finite element approximation must now be defined also for the membrane strain components $[\bar{E}^0]$ (see equations (15)). According to the notations introduced in equations 31, we have :

$$[\bar{E}^0] = \begin{bmatrix} \epsilon^0{}_{\xi\xi} \\ \epsilon^0{}_{\eta\eta} \\ \epsilon^0{}_{\xi\eta} \\ \epsilon^0{}_{\eta\xi} \end{bmatrix} = \begin{bmatrix} v_{\xi,\xi} - b_{11}v_3 \\ v_{\eta,\eta} - b_{22}v_3 \\ v_{\xi,\eta} - b_{12}v_3 \\ v_{\eta,\xi} - b_{21}v_3 \end{bmatrix} \tag{35}$$

As previously stated for transverse shear strains, membrane strain interpolations coming from the isoparametric approach have to be removed and consistently assumed in order to improve the shell finite element behavior. Actually, from the above sections it is easy to show that derivatives appearing in

equation (35) are incompleted second order polynomia, v_3 being a third order one. Therefore, the only way to have the same polynomia for the interpolation of the vector ϵ^0 is to choose the following set of monomial terms : $\{1, \xi, \eta, \xi\eta\}$.

This polynomial base involves choosing four points to evaluate each membrane strain component : two in the ξ direction and two in the η direction. Numerical plate membrane tests with distorded meshes indicate that the best choice is that given by the reduced integration points denoted by $K_1, \ldots, K_4$ (see Figure 3).

The interpolation of the membrane strain components can be written as the matrix product :

$$\left[\tilde{E}^0\right] = [BM]\,[PM]\,[ql_e] \tag{36}$$

with

$$[PM]\,[ql_e] = \left[\begin{array}{cccccccc} \epsilon^0_{\xi\xi}(K_1) & \ldots & \epsilon^0_{\xi\xi}(K_4) & \epsilon^0_{\eta\eta}(K_1) & \ldots & \epsilon^0_{\eta\eta}(K_4) \\ \epsilon^0_{\xi\eta}(K_1) & \ldots & \epsilon^0_{\xi\eta}(K_4) & \epsilon^0_{\eta\xi}(K_1) & \ldots & \epsilon^0_{\eta\xi}(K_4) \end{array}\right]^T$$

$$[BM] = \left[\begin{array}{cccc} [C\xi\eta] & [0] & [0] & [0] \\ [0] & [C\xi\eta] & [0] & [0] \\ [0] & [0] & [C\xi\eta] & [0] \\ [0] & [0] & [0] & [C\xi\eta] \end{array}\right]$$

$$\text{and where} \quad [C\xi\eta] = \left[\begin{array}{ccc} C\xi\eta_{K1}(\xi,\eta) & \ldots & C\xi\eta_{K4}(\xi,\eta) \end{array}\right]$$

In this expression, subscripts K_{1-4} indicate the points where membrane strain components are evaluated (see Figure 3) and $C\xi\eta_K$ are defined as follows :

$$\begin{aligned} C\xi\eta_{K1}(\xi,\eta) &= (1-\sqrt{3}\xi)(1-\sqrt{3}\eta)/4 \\ C\xi\eta_{K2}(\xi,\eta) &= (1+\sqrt{3}\xi)(1-\sqrt{3}\eta)/4 \\ C\xi\eta_{K3}(\xi,\eta) &= (1+\sqrt{3}\xi)(1+\sqrt{3}\eta)/4 \\ C\xi\eta_{K4}(\xi,\eta) &= (1-\sqrt{3}\xi)(1+\sqrt{3}\eta)/4 \end{aligned}$$

4.4. About the degenerated approach

The same finite element approximations have been used for the degenerated approach. From the generalized strain components given in equations (18), we construct an isoparametric approximation for the bending part, and an assumed strain approximation for membrane and shear parts. The methodology is the same as above for the finite element based on the curvilinear shell model.

4.5. The other assumed strain 8 node elements

A comparison for shear and membrane strain approximations can be made with the two other 8 nodes listed in Section 1.. These two elements are based on the degenerated approach.

For the MITC8 element (see Reference [Bat86]), shear strain is defined from six point evaluations for each component, while membrane strain is based on six

point evaluations for the two extension components and four point evaluations for in-surface shear components.

In Reference [Hua86], five point evaluations are used for the shear and membrane strain approximations. It must be denoted that the membrane strain is expressed in a local cartesian co-ordinate system and the interpolation used for the transverse displacement is isoparametric.

From those remarks, differences in the way of approximating the strain are clear between our method and other eight nodes : we use a cubic transverse displacement interpolation with a tangential shear strain constraint on the edges of the element. Five point evaluations are then used for the shear strain approximation and four point evaluations for the membrane strains.

5. Numerical Evaluations

In this section, classic membrane and shell problems are taken from the litterature so as to test this new shell finite element, denoted M2D. A third rotation is introduced in order to project the dof in the cartesian co-ordinate system. For each test, a comparison is presented between this finite element based on a doubly curved shell theory and the finite element based on the well known degenerated approach, denoted MDG. The stiffness matrix of these two finite elements are obtained using a 3×3 Gauss integration scheme.

Above all, the eigenvalues have been computed in a plate configuration with a one element mesh and we have got seven zero eigenvalues. This finite element exhibits one spurious mode which is not communicable.

The finite element presented in this work passes the membrane and bending (see reference [Pol94]) patch-test of reference [Mac85].

Two plate tests to evaluate the in-plane membrane strain finite element approximations, and three classical shell problems are presented in this Section.

A remark can be made about the membrane behaviour of these shell problems (see Reference [Cha98]) : only the hemispherical shell is a membrane locking test named non-inhibited pure bending, where membrane strain is negligible in comparison with the bending strain. The two others (the Scordelis-Lo roof and the pinched cylinder) are inhibited bending tests and are good for evaluating the ability of a shell finite element to represent a complex membrane strain state.

5.1. The straight cantilever beam problem

This test is described in Figure 4. We compare the membrane approximation presented in this work with isoparametric ones. Results obtained for curved and degenerated finite elements are indicated in Table 1 and show good agreement with reference values given in Reference [Mac85].

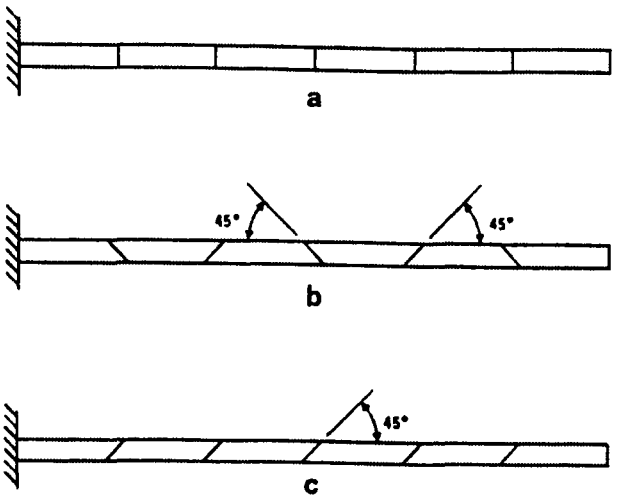

Figure 4: *Straight cantilever beam problem : Lenght* = 6.0 , *width* = 0.2 , e = 0.1 , E = 1.e7 , ν = 0.3 ; *mesh* = 6 × 1 : *(a) regular shape elements, (b) trapezoidal shape elements, (c) parallelogram shape elements ; boundary condition : clamped edge for* $x_1 = 0$ *; loading : unit forces at free end*

	ISOPARAMETRIC	present membrane strain approximation (MDG-M2D)
Extension		
a)	.2994	.2999
b)	.2994	.2995
c)	.2994	.2996
In-plane shear		
a)	.1062	.1067
b)	.0972	.1048
c)	.1059	.1066
Reference value for the extension : 0.3		
Reference value for the in-plane shear : 0.1081		

Table 1: *Straight cantilever beam problem for three meshes : a) rectangular elements, b) trapezoidal elements, c) parallelogram elements ; value at the center point of the free edge for* v_1 *(extension case) and* v_2 *(in-plane shear case)*

5.2. Cook's membrane problem

The description of this test is shown in Figure 5. Results are given in Table 2 and show a better behaviour for our membrane strain approximation than for the isoparametric one in comparison with reference value from Reference

[Sim89].

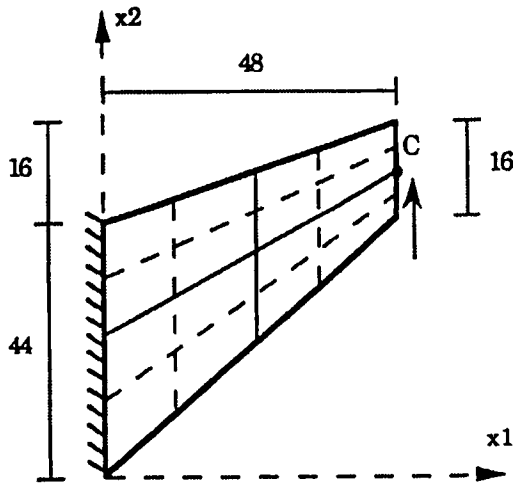

Figure 5: *Cook's membrane problem : dimensions are indicated on the figure ;* $e = 1.0$, $E = 1.0$, $\nu = 0.333$ *; different meshes* ($N = 1, 2, 4$) *are presented in the figure ; boundary condition : clamped edge for* $x_1 = 0$ *; loading : unit force at free end*

N	ISOPARAMETRIC	present membrane strain approximation (MDG-M2D)
1	17.22	19.14
2	22.72	23.10
4	23.71	23.72
Reference value :	23.90	

Table 2: *Cook's membrane problem ; value of* v_2 *at the point* C

5.3. Scordelis-Lo roof

This test is presented in Figure 6, and considering the symmetry of the problem only one quarter of the roof is analyzed (part $ABCD$). This is the first shell test and results are presented in Table 3 for the vertical displacement at the midpoint B of the free edge and at the center C of the roof.

The behaviour of the two finite elements is identical for this test : at point B, the same value is obtained for the $N = 2$ mesh while at point C, it is for the $N = 4$ mesh. These values are in good agreement with reference values.

Convergence velocity is good compared to other kinds of finite elements (4 and 9 nodes), see Reference [Bat92].

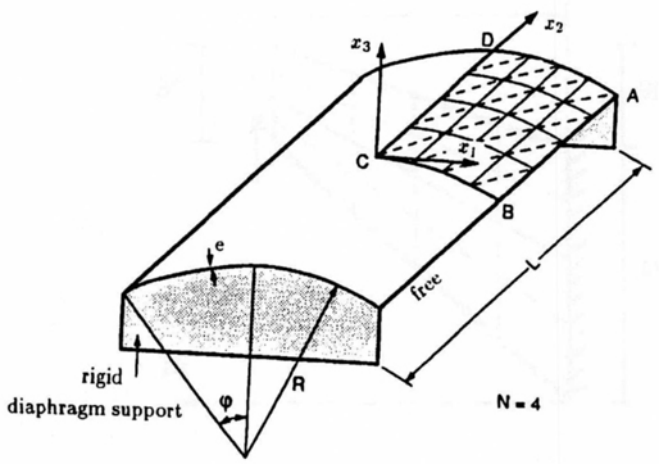

Figure 6: *Scordelis-Lo roof problem :* $L = 6.0$, $R = 3.0$, $e = 0.03$, $\phi = 40.0$, $E = 3.e10$, $\nu = 0.0$ *; the mesh* $= 4 \times 4$ $(N = 4)$ *is presented in the figure ; gravity load* $= 0.20833$

N	dof	$-v_3e1$ at B		v_3e2 at C	
		M2D	MDG	M2D	MDG
1	24	.195	.343	.251	.732
2	84	.360	.359	.584	.574
4	312	.361	.361	.545	.545
8	1200	.361	.361	.542	.542
10	1860	.361	.361	.542	.542
Reference value at B : -.361e-1					
Reference value at C : .541e-2					

Table 3: *Scordelis-Lo roof problem ; value of* v_3 *at the point* B *and* C

5.4. Pinched cylinder

This test is shown in Figure 7, and considering the symmetry of the problem only one eighth of the cylinder was analyzed (part $ABCD$).

Results are presented in Table 4 for the normal displacement at the center C and for the axial membrane displacement at the point D on the rigid diaphragm.

From Table 4, one can see that convergence is less rapid than for the Scordelis-Lo roof test presented above. This is due to the loading which is a pointwise transverse force. Same values for the curved and degenerated shell approaches are reached for the $N = 4$ mesh at point C and $N = 8$ at point D.

At point D (see $N = 2$), we can observe that the DG element presents an oscillation for the membrane displacement while M2D has a monotone convergence.

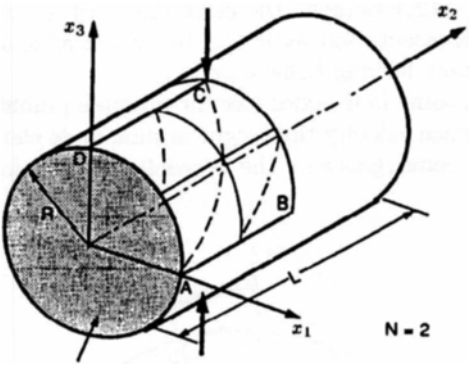

Figure 7: *Pinched cylinder problem : $L = 6.0$, $R = 3.0$, $e = 0.03$, $E = 3.e10$, $\nu = 0.3$; the mesh ($N = 2$) is presented in the figure ; unit point load at the two opposite points*

N	dof	$-v_3e6$ at C		v_2e8 at D	
		M2D	MDG	M2D	MDG
1	18	.009	.012	.064	.101
2	72	.121	.130	.443	.737
4	288	.171	.172	.470	.427
8	1152	.184	.183	.458	.457
10	1800	.183	.182	.458	.457
Reference value at C : -.182e-6					
Reference value at D : .457e-8					

Table 4: *Pinched cylinder problem ; value of v_3 at the point C and value of v_2 at the point D*

5.5. Hemispherical shell

This test is described in Figure 8. Considering the symmetry of the problem, only one quarter of the hemispherical shell has been analyzed (part $ABCD$).

The results obtained for the two finite elements are given in Table 5. The same value is reached for the transverse displacement at point A for the $N = 8$ mesh.

Some comments must be made on this test : the boundary conditions are minimum to avoid rigid body motions and, as above for the pinched cylinder, two pointwise transverse forces are defined.

The convergence is different for the two finite elements but the convergence value is reached for the same mesh. Therefore, a finite element based on a doubly curved shell model gives as good a result as the classic degenerated approach. The M2D element therefore does not present a problem of rigid body motion representation as it can be read classically and does not show stronger membrane locking behaviour.

On this test, some four nodes (see for example [Sim89] and [And93]) have a quicker convergence velocity than eight or nine node elements but they present a lower velocity convergence on the Scordelis-Lo roof, for example.

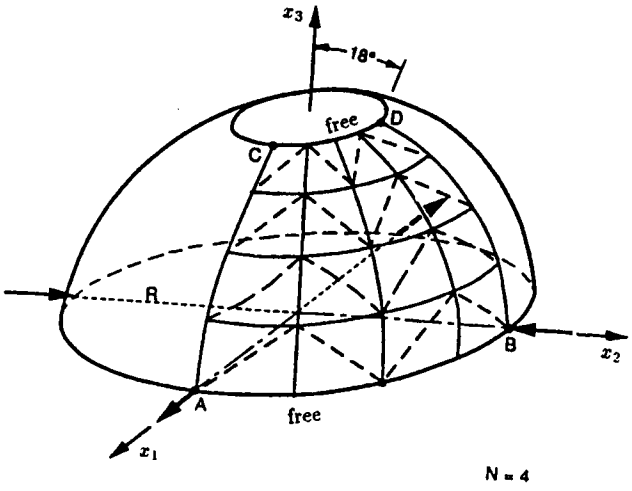

Figure 8: *Hemispherical shell problem :* $R = 10.0$, $e = 0.04$, $E = 6.825e7$, $\nu = 0.3$ *; the mesh* ($N = 4$) *is presented in the figure ; point load* $= \pm 2.0$ *at the four opposite points*

5.6. Helical shell

This test is described in Figure 9 and has been firstly proposed by [Mac85] and is now considered as a reference shell test in [Bat92]. It allows, in the case of explicit integration through the thickness (see (22) and (23)), to control the efficiency of those integrations for the strain approximations.

N	dof	$v_1 e1$ at A	
		M2D	MDG
1	29	.300	.942
2	95	.050	.170
4	335	.725	.790
8	1247	.929	.931
10	1919	.933	.934
Reference value at A : .940e-1			

Table 5: *Hemispherical shell problem ; value of* v_1 *at the point A*

The results obtained by the two finite elements are given in Table 6. Two thicknesses ($e = 0.32$ and $e = 0.0032$) are considered and two point load directions are tested. Reference solutions are obtained from the beam theory [Bat92].

Only one mesh results are presented (N = 2 × 12 with 576 dof) and results are in good agreement with reference solutions for the two shell finite elements and for the different thicknesses and load cases.

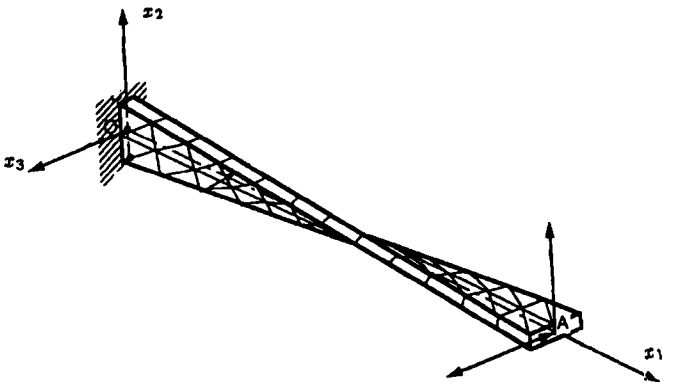

Figure 9: *Helical shell problem :* $L = 12.0$, *width* $= 1.1$, *twist* $= 90$ deg *(root to tip),* $E = 29.e6$, $\nu = 0.22$ *; the mesh (*$N = 2 \times 12$*) is presented in the figure ; point forces on A (in-plane and out-plane load)*

6. Conclusion

The main basic feature of this work is in the development of a new eight node shell finite element (M2D) based on a doubly curved shell theory. From this work we can observe that :

type of load	M2D	MDG	ref. values
In-plane		v_3 at A	
$e = 0.32$ and $F = 1.e3$	5.42	5.41	5.42
$e = 0.0032$ and $F = 1.$	5211	5218	5316
Out-of-plane		v_2 at A	
$e = 0.32$ and $F = 1.e3$	1.75	1.75	1.75
$e = 0.0032$ and $F = 1.$	1293	1291	1296

Table 6: *Helical shell problem ; value at the point A for the* $N = 2 \times 12$ *mesh*

- the way to construct this finite element (M2D) is the same as for (DG) based on the degenerated approach, differences are in the way of defining the in-surface displacement vector.
- results from (M2D) and (DG) elements are then of the same order for convergence velocity and accuracy for the four classic shell tests.

There is in fact no reason to oppose the two approaches to obtain finite elements : the (M2D) element presents no problem of rigid body mode representation, and (M2D) and (DG) elements present together the same transverse shear and membrane locking defaults.

The methodology presented for plates (see Reference [Pol94]) to avoid shear locking is extended with success to shells, and in the same spirit, the technique used for the membrane strain gives good results for a reasonable ratio length/thickness. The membrane locking is controlled but we cannot say, as for the shear locking, that it has fully disappeared, because for a very thin shell the convergence velocity is slower.

Finally, the shear locking has completely disappeared for plate and shell structures but it seems that membrane locking needs more work to be completely avoided. Future work is therefore directed towards the understanding of membrane locking and to an improvement of velocity convergence using curved or degenerated shell elements for the pinched cylinder and hemispherical shell.

Acknowledgements

A part of this work has been supported by the Research Department of Renault, 92500 Rueil-Malmaison (France), and is also the Doctoral Thesis of the first author [Pol92].

References

[Ahm70] S. Ahmad, B.M. Irons, and O.C. Zienkiewicz. Analysis of thick and thin shell structures by curved elements. *Int. Jour. Num. Meth. Eng.*, 2:419–451, 1970.

[And93] U. Andelfinger and E. Ramm. Eas-elements for two dimensional, three dimensional, plate and shell structure and their equivalence to hr-element. *Int. Jour. Num. Meth. Eng.*, 36:1311–1337, 1993.

[Buc93] M.L. Bucalem and K.-J. Bathe. Higher-order mitc general shell elements. *Int. Jour. Num. Meth. Eng.*, 36:3729–3754, 1993.

[Bat86] K.-J. Bathe and E.N. Dvorkin. A formulation of general shell elements - the use of mixed interpolation of tensorial components. *Int. Jour. Num. Meth. Eng.*, 22:697–722, 1986.

[Bat92] J.L. Batoz and G. Dhatt. *Modelling of structures by finite elements.* Hermès, Paris, 1992. (in french).

[Bue92] N. Buechter and E. Ramm. Shell theory versus degeneration – a comparison in large rotation finite element analysis. *Int. Jour. Num. Meth. Eng.*, 34:39–59, 1992.

[Bab92] I. Babuska and M. Suri. On locking and robustness in the finite element method. *SIAM Jour. Numer. Anal.*, 51:221–258, 1992.

[Bel85] T. Belytschko, H. Stolarski, W.K. Liu, N. Carpenter, and J.S.-J. Ong. Stress projection for membrane and shear locking in shell finite elements. *Comp. Meth. Applied Mech. and Eng.*, 51:221–258, 1985.

[Cha98] D. Chapelle and K.J. Bathe. Fundamental considerations for the finite element analysis of shell structures. *Comp. and Struc.*, 66(1):19–36, 1998.

[Coo74] R.D. Cook. *Concepts and Applications of Finite Element Analysis.* J. Wileys and Sons, New-York, 1974.

[Gil91] W. Gilewski and M. Radwanska. A survey of finite element models for the analysis of moderately thick shells. *Finite Elements in Analysis and Design*, 9:1–21, 1991.

[Hin86] E. Hinton and H.C. Huang. A family of quadrilateral mindlin plate elements with substitute shear strain fields. *Comp. and Struc.*, 23(3):409–431, 1986.

[Hua86] H.C. Huang and E. Hinton. A new nine node degenerated shell element with enhanced membrane strain interpolation. *Int. Jour. Num. Meth. Eng.*, 22:73–92, 1986.

[Ide81] S. Idelsohn. On the use of deep, shallow or flat shell finite elements for the analysis of thin shell structures. *Comp. Meth. Applied Mech. and Eng.*, 26:321–330, 1981.

[Mac85] R.H. MacNeal and R.L. Harder. A proposed set of problems to test finite element accuracy. *Finite Elements in Analysis and Design*, 1:3–20, 1985.

[Mac92] R.H. MacNeal and R.L. Harder. Eight nodes or nine ? *Int. Jour. Num. Meth. Eng.*, 33:1049–1992, 1992.

[Noo89] A.K. Noor. List of books, monographs, conference proceeding and survey papers on shells. In Noor et al., editor, *Analytical and Computational Models of Shells*, volume 3, pages 7–33, 1989.

[Pin89] P.M. Pinsky and R.V. Jasti. On the use of bubble functions for controlling accuracy and stability of mixed shell finite elements. In Noor et al., editor, *Analytical and Computational Models of Shells*, volume 3, pages 359–382, 1989.

[Pol92] O. Polit. *Développement d'éléments finis de plaques semi-épaisses et de coques semi-épaisses à double courbure.* PhD thesis, University P. and M. Curie, Paris VI, 1992.

[Par89] K.C. Park, E. Pramono, G.M. Stanley, and H.A. Cabiness. The ans shell elements : earlier and recent improvements. In Noor et al., editor, *Analytical and Computational Models of Shells*, volume 3, pages 359–382, 1989.

[Pol94] O. Polit, M. Touratier, and P. Lory. A new eight-node quadrilateral shear-bending plate finite element. *Int. Jour. Num. Meth. Eng.*, 37:387–411, 1994.

[Sim89] J.C. Simo, D.D. Fox, and M.S. Rifai. On a stress resultant geometrically exact shell model. part ii : the linear theory ; computational aspects. *Comp. Meth. Applied Mech. and Eng.*, 73:53–92, 1989.

[San89] E. Sanchez-Palencia. Statique et dynamique des coques minces. i. cas de flexion pure non inhibée. *C.R. Acad. Sci. Paris*, t.309:411–417, 1989.

[Wem89] G. Wempner. Mechanics and finite elements of shells. *App. Mech. Rev.*, 42(5):129–142, 1989.

[Yan90] H.T.Y. Yang, S. Saigal, and D.G. Liaw. Advances of thin shell finite elements and some applications - version i. *Comp. and Struc.*, 35(4):481–504, 1990.